State-of-Health Estimation Based on Differential Temperature for Lithium Ion Batteries

Jinpeng Tian, *Student Member, IEEE*, Rui Xiong, *Senior Member, IEEE*, and Weixiang Shen, *Senior Member, IEEE*

***Abstract*—State-of-health (SOH) estimation is necessary for lithium ion batteries due to ineluctable battery ageing. Existing SOH estimation methods mainly focus on voltage characteristics without considering temperature variation in the process of health degradation. In this article, we propose a novel SOH estimation method based on battery surface temperature. The differential temperature curves during constant charging are analyzed and found to be strongly related to SOH. Part of the differential temperature curves in a voltage range is adopted to establish a relationship with SOH using support vector regression. The influence of battery discrepancy, voltage range, and sampling step are systematically discussed and the best combination of voltage range and sampling step is determined using leave-one-out validation. The proposed method is then validated and compared with an incremental capacity analysis (ICA)-based SOH estimation method using the Oxford and NASA datasets, which were collected from different cells under different conditions, respectively. The results show that the proposed method is capable of estimating SOH with the root-mean-square error less than 3.62% and 2.49%, respectively. In addition, the proposed method can improve the overall SOH estimation accuracy and robustness by combining with the ICA-based method with little computational burden.**

***Index Terms*—Battery ageing, battery management, differential temperature, lithium ion battery, state-of-health.**

I. Introduction

A. Literature Review

LITHIUM ion batteries are one of the most attractive energy storage systems in various applications. However, irreversible health degradation poses significant challenges in battery management [1]. As capacity fade is strongly related to battery life, state-of-health (SOH) is usually defined as a ratio of present capacity to initial capacity. Different from state of charge (SOC) estimation, which primarily relies on open-circuit voltage (OCV) [2], [3], there is no consensus among researchers regarding a well-accepted parameter that can reflect battery SOH. Hence, SOH estimation boils down to finding a health indicator (HI) which can be readily acquired with measured signals and is sensitive to SOH variation. The SOH is then estimated by feeding the measured or identified HI to the SOH estimator established using experimental data.

As an electrochemical power source, lithium ion batteries have the salient feature in the terminal voltage, from which a set of HIs have been acquired. Studies on battery ageing mechanisms revealed that loss of active materials and loss of Li-ion inventory can increase impedance [4] and affect polarization voltage. In the frequency domain, electrochemical impedance spectroscopy (EIS) has been widely used to characterize impedance and estimate SOH. Tröltzsch *et al.* [5] found the SOH fade is a monotonic function of charge transfer resistance, double-layer capacity and Warburg coefficient of an impedance model. Zhou *et al.* [6] determined three specific frequencies at which the impedance can be utilized to estimate SOH. Nevertheless, the stringent requirements for EIS tests hinder the application of the impedance to SOH estimation. To circumvent this problem, researchers fell back on time-domain identification. Ohmic resistance [7], polarization resistance [8], polarization capacitance [9], solid-state diffusion coefficient [10], and OCV [11] have been identified from dynamic discharging profiles to estimate SOH. Some other HIs were found without electrochemical mechanisms, such as the sample entropy of dynamic voltage responses [12]. However, these HIs require consistent discharging profiles, and further validation on unpredictable discharging profiles is still an open question [13].

On the other hand, battery charging modes are usually controllable and therefore provide valuable data for SOH estimation. In particular, the simple constant-current charging method is widely applied [14]. The incremental capacity analysis (ICA) [15] has also been implemented into battery management systems (BMSs) for SOH estimation using voltage curves during constant-current charging. Weng *et al.* [16] demonstrated that the SOH can be estimated by tracking the height of incremental capacity (IC) peaks. Thereafter, peak position [17] and area [18] were also reported to be promising HIs. However, the ICA theory was developed based on OCV data which are usually obtained through 1/25 C charging/discharging [15]. Its application under higher rate charging conditions (e.g., 1 C in [18]) needs

Manuscript received December 2, 2019; revised February 2, 2020; accepted February 28, 2020. Date of publication March 5, 2020; date of current version June 23, 2020. This work was supported by the National Natural Science Foundation of China under Grants 51877009 and 51922006. Recommended for publication by Associate Editor G. Oriti. *(Corresponding author: Rui Xiong).*

Jinpeng Tian is with the Department of Vehicle Engineering, School of Mechanical Engineering, Beijing Institute of Technology, Beijing 100081, China, and also with the Faculty of Science, Engineering and Technology, Swinburne University of Technology, Melbourne, VIC 3122, Australia (e-mail: jtian@swin.edu.au).

Rui Xiong is with the Department of Vehicle Engineering, School of Mechanical Engineering, Beijing Institute of Technology, Beijing 100081, China (e-mail: rxiong@bit.edu.cn).

Weixiang Shen is with the Faculty of Science Engineering and Technology, Swinburne University of Technology, Melbourne, VIC 3122, Australia (e-mail: wshen@swin.edu.au).

Color versions of one or more of the figures in this article are available online at http://ieeexplore.ieee.org.

Digital Object Identifier 10.1109/TPEL.2020.2978493

further theoretical support. In addition, as the reciprocal of the differential voltage is applied, sampling noise is significantly amplified [18].

It is noteworthy that the above-mentioned studies extensively depend on voltage characteristics of batteries, while the other sources of information are neglected. Recent research has shown that the signals like temperature [19], [20], force [21], and ultrasound [22] are capable of characterizing battery ageing from different aspects. Extracting HIs from different sources of information is beneficial to the accuracy and robustness of the SOH estimation. In particular, temperature is an important parameter which is usually monitored for thermal management [23]. Pecht *et al.* [24] have revealed that temperature is a critical cause of many failure modes. To further study the influence of ambient temperature on battery ageing, an electrochemistry-based model was applied in [25] to simulate ageing behaviors over the temperature range of 25 to 55 °C. Results showed that batteries underwent significant film formation and modification, and even structural/phase changes at elevated temperatures. In addition, battery heat generation significantly depends on the current rate and cell design [26]. To reduce heat generation rate, Zhang *et al.* [27] established an electrochemical–electrical–thermal model in COMSOL, and the cell tab arrangements were optimized. Above studies highlighted the importance of temperature on battery management and tried to control the temperature to ensure safe and reliable operation of batteries. On the other hand, the sampled temperature is also a critical information source that can facilitate state estimation. Mejdoubi *et al.* [28], [29] have systematically demonstrated that incorporating surface temperature variation into a model-based SOC and SOH estimation method can enhance accuracy and robustness. In their work, temperature compensation was considered during parameter identification and state estimation while the surface temperature was not directly considered as input. Wu *et al.* [19] analyzed battery ageing mechanisms based on battery surface temperature and concluded that temperature variation is conducive to providing information about entropic change. In addition, it is suitable for high-rate charging than the ICA method which is theoretically based on OCV measurement. In their ingenious work, the conventional ICA method was augmented by accounting for temperature variation, resulting in differential thermal voltammetry (DTV) method. Although the peaks in the DTV curves have been reported to be tightly related to battery degradation [19], differentials of both temperature and voltage together will inevitably lead to difficulties in the data processing. Particularly, the DTV data are vulnerable to disturbance in the voltage measurement as the differential voltage appears in the denominator.

B. Contributions

Focusing on the problems mentioned above, this article devotes to the development of a novel SOH estimation method which takes advantage of battery surface temperature. Its main contributions are listed as follows.

1) Temperature-based SOH estimation: A novel SOH estimation method utilizing the differential temperature (DT) is proposed. The DT curves are extracted from surface temperature and show a clear dependence on SOH fade. An SOH-sensitive region is determined on the DT curves. The data in this region are then sampled and fed into the support vector regression algorithm to estimate SOH.
2) Systematic validation on two datasets: The proposed method is validated on two datasets collected from different cells under different conditions. The impact of battery discrepancy, voltage range, and sampling step on SOH estimation is investigated through leave-one-out validation. Results show the root-mean-square error (RMSE) is within 3.62% and 2.49% for two datasets, respectively.
3) Combination with the ICA method: A combination framework is proposed to enhance the overall performance of SOH estimation. Through combining the proposed DT-based method with a widely used ICA method, the overall estimation accuracy is improved and the combination is promising to ensure the robustness.

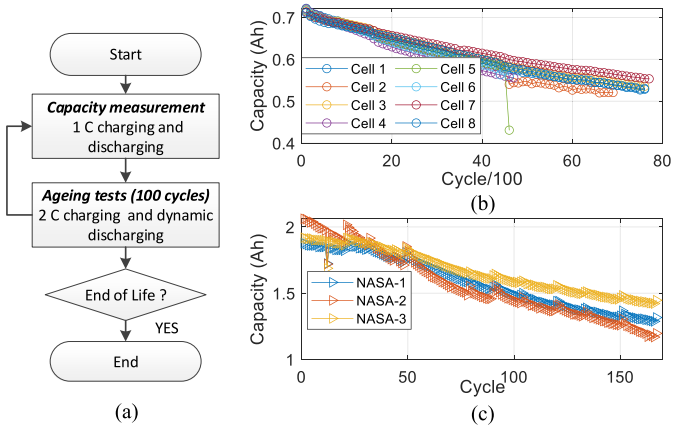

Fig. 1. (a) Test schedule for the Oxford dataset. (b) Capacity evolution of eight cells in the Oxford dataset. (c) Capacity evolution of three cells in the NASA dataset.

C. Article Organization

The rest of the article is organized in the following manner. The employed datasets are introduced in Section II, and the proposed SOH estimation method is then described in Section III. Detailed validation and combination with the ICA method are discussed in Section IV. Finally, the conclusion is drawn in Section V.

II. Battery Degradation Datasets

A. Oxford Dataset

The Oxford battery degradation dataset [30], [31] includes battery ageing data collected from eight Kokam pouch cells with a nominal capacity of 740 mAh. They are labeled as cell 1 to cell 8 in this article, respectively. The cathode material of the cells is lithium cobalt oxide and lithium nickel cobalt oxide. The anode material is graphite. As shown in Fig. 1(a), in the ageing test, eight cells were repeatedly charged at 2 C and discharged using a dynamic profile to simulate automotive

applications [32]. Every 100 ageing cycles, a 1 C charging and discharging cycle was conducted to measure battery capacity. Current, voltage, and surface temperature were recorded with 1 s intervals by a Bio-Logic MPG-205 battery tester at 40 °C, regulated by a Binder thermal chamber. In this study, the 1 C charging data are adopted for the development and validation of the SOH estimation method. Battery capacity can be computed by integrating the current over the charging period. Thereafter, the SOH can be calculated by

$$\begin{cases} C_a = \int_0^{t_f} \eta I(\tau)\, d\tau \\ \text{SOH} = C_a / C_{a,0} \end{cases} \tag{1}$$

where $I(\tau)$ and t_f stand for current and total charging time, respectively. η is the coulombic efficiency, which is set to 1 for lithium ion cells. C_a is the current capacity of a battery, whose initial capacity is $C_{a,0}$. The capacity evolution of the eight cells is plotted in Fig. 1(b), and it contains more than 500 capacity measurements, covering an SOH range greater than 40%. In a few tests, the sampled surface temperature is far from 40 °C, e.g., it is around 0 °C, and such data are not used in the sequel.

B. NASA Dataset

Another public battery degradation dataset from NASA [33] is also employed in this work. It contains battery degradation data from three 18 650 cells with $LiNi_{0.8}Co_{0.15}Al_{0.05}O_2$ cathode and graphite anode, and the cell nominal capacity is 2 Ah. They are labeled as NASA-1, NASA-2, and NASA-3 in the present work, respectively. In the ageing test, these three cells were repeatedly charged in a constant-current–constant-voltage mode at 1.5 A to 4.2 V, and the cut-off current was 20 mA. Then, 2 A current was applied to discharge the cells to 2.7, 2.5, and 2.2 V, respectively. During the test, the cells were kept at the room temperature ($\sim$24 °C) and the current, voltage, and surface temperature were sampled by an Arbin tester. The capacity degradation path is generated from the ageing test based on (1), and the results are shown in Fig. 1(c).

In the present study, the Oxford dataset which contains more data from more cells is used as the primary dataset for the development, analysis, and validation of the SOH estimation method. On the other hand, the charging data from the NASA dataset are applied as another case study to further validate the proposed SOH estimation method.

III. SOH Estimation Method

This section outlines the development of the proposed SOH estimation method based on cells 1–8 from the Oxford dataset. First, the procedure to obtain the DT curves is elucidated. Then, the ability of DT curves for ageing diagnosis and SOH estimation is analyzed. After that, the HI is extracted from the DT curves for regression.

A. Procedure to Calculate DT Curves

In view of the limited resolution of temperature sensors, direct calculation of the DT is vulnerable to measurement noise. To circumvent this issue, the DT curves are approximated using finite difference over L sampling intervals, which is expressed as follows:

$$DT_m(k) = \frac{dT}{dt}(k) \approx \frac{T(k) - T(k-L)}{L}. \tag{2}$$

A large L corresponds to a large temperature variation over the L sampling intervals, therefore it can reduce the influence of measurement noise. On the other hand, subtle DT variation may not be captured if L is too large. In the present study, we select $L = 20$ s for the adopted datasets according to our experience, and its selection for other experimental data depends on the quality of temperature measurement. The Kalman filter listed in Table I is implemented to further smooth the obtained DT curves [18]. In this regard, the smoothed DT value is considered as a state polluted by random noise $w(k)$ and $v(k)$

$$\begin{cases} \text{DT}(k) = \text{DT}(k-1) + w(k-1) \\ \text{DT}_m(k) = \text{DT}(k) + v(k). \end{cases} \tag{3}$$

The obtained DT curves of cell 1 are plotted in Fig. 2 as a function of the terminal voltage. These curves can be separated into three regions, termed Region I, II, and III, respectively, since the DT curves in these regions show different trends as SOH fade. In Region I (<3.6 V), the DT curves slightly move to the right and the amplitude increases when the voltage approaches 3.6 V. Some outliers appear at the initial five capacity tests due to the discrepancy in initial temperature at these cycles. A possible reason for this is the setting of the thermal chamber. After the beginning of battery charging, such phenomenon gradually disappears as battery heating dominates the DT curves [19]. There exists a consistent peak around the voltage of 3.8 V, and on its right, the variation of DT curves in Region III (>3.8 V) is more regular but is not very apparent. In contrast, in

TABLE I
Procedure of the Kalman Filter

Definition:

$$\begin{cases} x(k) = Ax(k-1) + w(k-1) \\ y(k) = Hx(k) + v(k) \end{cases}$$

where y is the measurement of x. w and v represent the process noise and measurement noise, with their covariance being Q_f and R_f, respectively. The state error covariance is defined as P. The Kalman gain is defined as K. The subscript k denotes the kth discrete time instant.

Initialisation:

Pre-set Q_f, R_f and the initial value of x and P.

Step 1 Prediction:

$$\begin{cases} x^-(k) = Ax(k-1) \\ P^-(k) = AP^-(k-1)A^T + Q_f \end{cases}$$

Step 2 Update:

$$\begin{cases} K(k) = P^-(k)H\left[HP^-(k)H^{\mathrm{T}} + R_f\right]^{-1} \\ x(k) = x^-(k) + K(k)\left[y(k) - Hx^-(k)\right] \\ P(k) = P^-(k) - K(k)HP^-(k) \end{cases}$$

k=k+1. Go to **Step 1**.

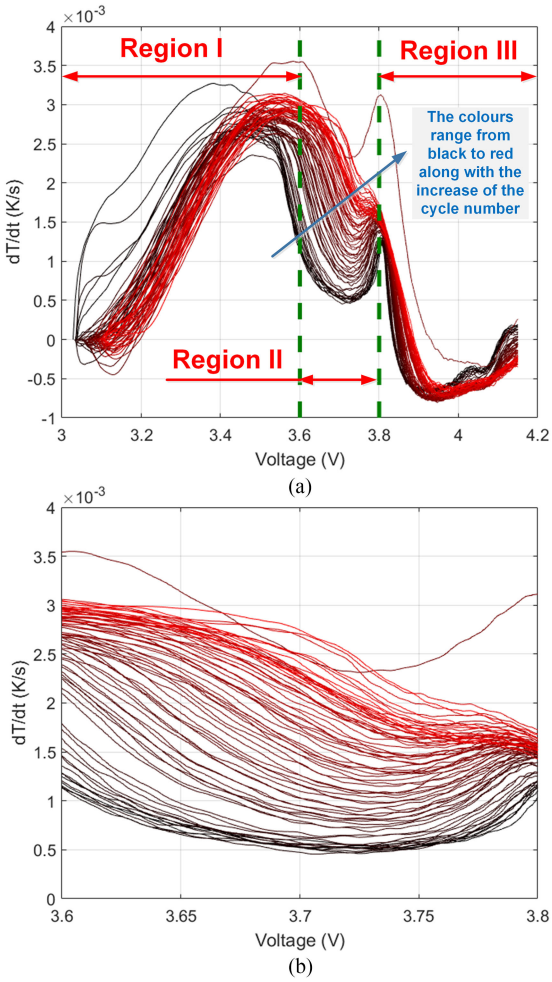

Fig. 2. (a) Obtained DT curves of cell 1. (b) Enlarged view of Region II. The colors range from black to red along with the increase of the cycle number.

Region II (3.6–3.8 V), DT curves show a monotonic and clear trend as SOH decreases. The behaviors of the DT curves, especially the DT curves in Region II are conducive to the study of ageing mechanisms and SOH estimation.

B. Qualitative Analysis of DT Curves

It should be underlined that although there exists a difference between internal and surface temperature, such difference is limited for daily constant-current charging, and the temperature distribution is usually assumed to be uniform [20]. Based on this assumption, the DTV method [19] has demonstrated its effectiveness in revealing inner mechanisms. In this section, the reason why DT curves are associated with battery ageing is discussed. The overall heat generation inside the batteries is composed of Joule heat and reaction heat, and the DT can be modeled as follows [20]:

$$\mathrm{DT} = \frac{1}{m_c c_p}\left(I^2 R_i + \frac{IT}{nF}\Delta S - hA\left(T - T_{\mathrm{amb}}\right)\right) \tag{4}$$

where T is the temperature, and I is the current. R_i is the battery resistance, F is the Faraday constant, and n is the number of exchanged electrons. ΔS is the entropy change, which is a function of lithium stoichiometry in cathode and anode materials. m_c and A are the mass and surface area of the tested cells, respectively. c_p and h is the heat capacity and equivalent heat transfer coefficient, both of which are constant during battery charging [19], [20]. T_{amb} is the ambient temperature, which keeps constant during the battery tests. In this equation, $I^2 R_i$ represents the Joule heat caused by the cell resistance. $\frac{IT}{nF}\Delta S$ represents the reversible reaction heat which originates from the variation of entropic change of electrodes during the intercalation/deintercalation of Li ions. The term $hA(T - T_{\mathrm{amb}})$ models the heat exchange to the environment. It can be noted during the constant-current charging process, the variation of the DT is only attributed to the resistance R_{i} and entropy change ΔS.

As reported by Wu *et al.* [19], compared with impedance, entropic heat generation contributes more to the variation of the DT curves. Therefore, the salient variation in Region II is mainly attributed to the variation of ΔS. Maher *et al.* [34], [35] studied the ΔS variation of both electrodes during cyclic ageing of lithium cobalt oxide/graphite coin cells. In their experimental results, a peak appears around the OCV of 3.95 V, at the left of which the ΔS changes significantly. This behavior qualitatively coincides with the variation of DT curves in Region II. Maher *et al.* [34], [35] ascribed such behavior to the crystal structure changes in the cathode from two aspects: reversible phase transition and irreversible symmetry conversion. Therefore, a possible reason for the variation of DT curves in Region II is the loss of active materials in the cathode, which was found to be more pronounced than that in the anode for the Oxford dataset [31]. Consequently, it is promising to infer battery ageing mechanisms form the variation of the DT curves. However, since the cathode of the cells in the Oxford dataset is a blend of lithium cobalt oxide and lithium nickel cobalt oxide, an in-depth quantitative analysis of ageing mechanisms using the DT curves may require accurate measurement of the cathode composition and the entropy change of both electrodes [20], which requires more electro-thermal experiments. From an engineering viewpoint, the variation of the DT curves provides valuable information on SOH fade. In the sequel, we show that SOH can be estimated by tracking the changes of the DT curves.

C. Extraction of the Health Indicator

SOH estimation requires extraction of HIs from the DT curves to reflect the SOH fade. Commonly used HIs include geometric or statistical features, such as the distance of two specific points in [20] or sample entropy in [12]. However, as can be observed from Fig. 2(b), slight fluctuations still exist in the DT curves, and therefore such HIs are vulnerable to sampling noise. To circumvent this issue, we directly sample DT values in Region II as the HI to establish the mapping between DT curves and SOH. For a given sampling step ΔU and a given voltage range $[U_{\mathrm{l}}, U_{\mathrm{h}}]$, the DT is sampled at $[U_{\mathrm{l}}, U_{\mathrm{l}} + \Delta U, U_{\mathrm{l}} + 2\Delta U, \ldots, U_{\mathrm{l}} + n\Delta U]$, yielding an HI vector $\mathbf{h} = [\mathrm{DT}_1, \mathrm{DT}_2, \ldots, \mathrm{DT}_n]$, with $n = \frac{U_h - U_l}{\Delta U}$. For example, if $\Delta U = 10$ mV is applied, the DT is sampled at [3.6,

3.61, …, 3.8] V, resulting in an HI vector containing 21 DT values.

D. Regression and Performance Evaluation

After determining the HI, its relationship with SOH is established in this part. Commonly used methods include polynomial functions [11] and machine learning [36]. Considering that the HI is a vector, a memory efficient machine learning algorithm, the support vector regression (SVR) is taken as an example to portray the correspondence between DT and SOH. As a renowned machine learning algorithm for regression, SVR has been successfully utilized for SOH estimation [16], [37]. The goal of SVR is to establish the mapping between observed HI vector $\mathbf{h}$ and SOH as follows:

$$f(\mathbf{h}) = \mathbf{w}^T\mathbf{h} + b \tag{5}$$

where $\mathbf{w}$ and b are algorithm parameters. A training dataset $\mathbf{D} = \{(\boldsymbol{h}_1, Q_1), (\boldsymbol{h}_2, Q_2), \ldots (\boldsymbol{h}_m, Q_m)\}$ is provided to parameterize (5) by solving the following problem:

$$\min_{\mathbf{w},b} \frac{1}{2}\|\mathbf{w}\|^2 + C\sum_{i=1}^{m} \ell_\varepsilon \left[f\left(\mathbf{h}_i\right) - Q_i\right] \tag{6}$$

where Q stands for SOH, C is a regularization parameter. ℓ_ε is an ε-insensitive loss function, which is expressed as follows:

$$\ell_\varepsilon\left(z\right) = \begin{cases} 0, & \text{if } |z| \le \varepsilon \\ |z| - \varepsilon, & \text{otherwise.} \end{cases} \tag{7}$$

with ε being a parameter regulating the penalty. By introducing two slack variables ξ_i and $\hat{\xi}_i$, (6) can be rewritten as follows:

$$\min_{\mathbf{w},b,\xi_i,\hat{\xi}_i} \frac{1}{2}\|\mathbf{w}\|^2 + C\sum_{i=1}^{m}\left(\xi_i + \hat{\xi}_i\right)$$
$$\text{s.t.} \begin{cases} f\left(\mathbf{h}_i\right) - Q_i \le \varepsilon + \xi_i \\ Q_i - f\left(\mathbf{h}_i\right) \le \varepsilon + \hat{\xi}_i \\ \xi_i, \hat{\xi}_i \ge 0. \end{cases} \tag{8}$$

Using the method of Lagrange multipliers, we can obtain the solution

$$f(\mathbf{h}) = \sum_{i=1}^{m} (\hat{\alpha}_i - \alpha_i)\kappa\left(\mathbf{h}_i, \mathbf{h}\right) + b \tag{9}$$

where $\hat{\alpha}_i$ and α_i are Lagrangian multipliers obtained using the $\kappa(\mathbf{h}_i, \mathbf{h}_j)$ which is a kernel function mapping the input from the input space to a high dimensional space. The widely used radial basis function is adopted in this study, and it is expressed as follows:

$$\kappa\left(\mathbf{h}_i, \mathbf{h}_j\right) = \exp\left(\frac{-\|\mathbf{h}_i - \mathbf{h}_j\|}{2\gamma}\right) \tag{10}$$

where γ is a parameter. In this article, parameters C, γ, and ε are optimized by using the grid search algorithm.

The offline trained SOH estimator is expected to estimate SOH of batteries whose characteristics completely do not appear in the training dataset. Therefore, the leave-one-out validation scheme is adopted to give a fair evaluation of the established estimator. As shown in Fig. 3, the data of each cell serve as the test dataset in turn, while the data of the remaining seven cells form the training dataset $\mathbf{D}$ [38]. The trained estimator is used to estimate the SOH of the test dataset, and the results are compared with the measured SOH. Three metrics, namely the maximum absolute error (MAE), RMSE, and R-squared (R^2) are defined to assess the estimation results:

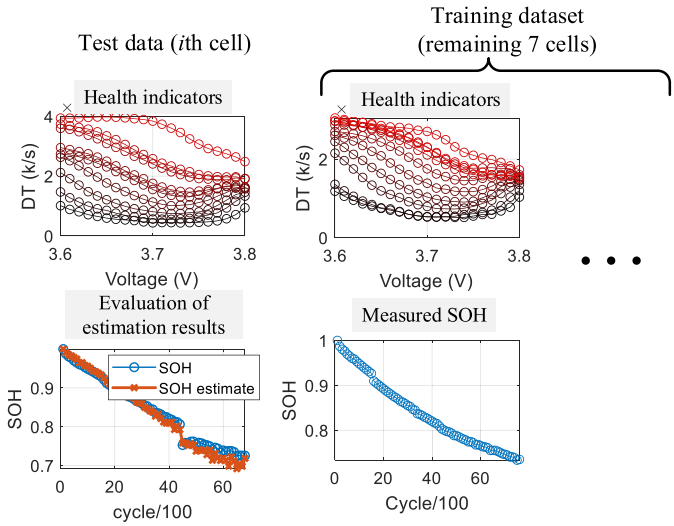

Fig. 3. Leave-one-out validation scheme.

$$\begin{cases} \text{MAE} = \max_{1\le i\le N}\left|\hat{Q}_i - Q_i\right| \\ \text{RMSE} = \sqrt{\sum_{i=1}^{N}\left(\hat{Q}_i - Q_i\right)^2/N} \\ R^2 = 1 - \sum_{i=1}^{N}\left(\hat{Q}_i - Q_i\right)^2 / \sum_{i=1}^{N}\left(\hat{Q}_i - \bar{Q}_i\right)^2 \end{cases} \tag{11}$$

where $\hat{Q}$ and $\bar{Q}$ represent the estimate and average of Q, respectively. N stands for the total number of capacity measurements in the test data. The MAE represents the largest estimation error, and the RMSE gives the standard deviation of the estimation errors. Both of them increase for worse estimation results. In contrast, R^2 represents the proportion of the variance for the estimated SOH that is explained by the input in the SOH estimator, with the ideal value being 1.

IV. Results and Discussions

In this section, the performance of the proposed method is validated. The influence of battery discrepancy, voltage range, and sampling step on the proposed method is discussed based on the Oxford dataset in detail, and the proposed method is also compared with the popular ICA-based SOH estimation method. Then, the proposed method is further validated on the NASA dataset. Finally, a case study is given to show the proposed method is able to be combined with the ICA method to achieve accurate and robust overall SOH estimation.

A. Validation on the Oxford Dataset

1) Influence of Battery Discrepancy: The proposed method is first directly conducted to estimate the SOH of all eight cells,

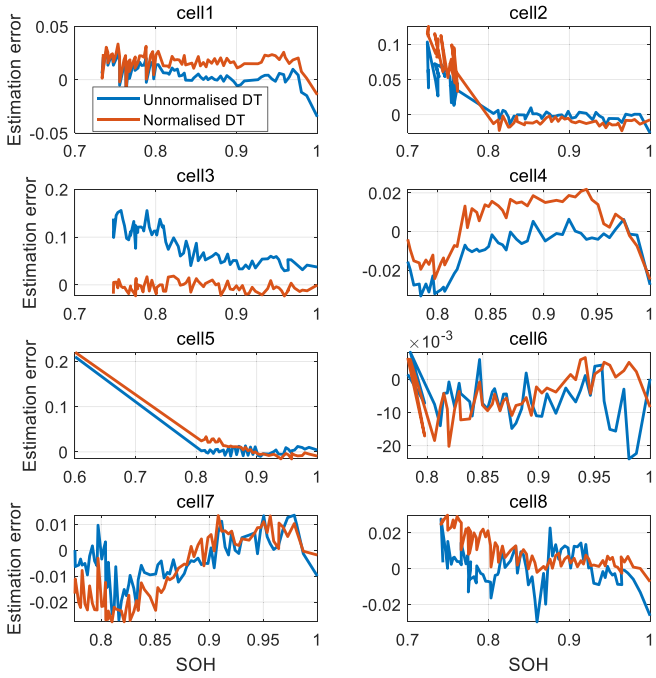

Fig. 4. SOH estimation errors for eight cells in the Oxford dataset.

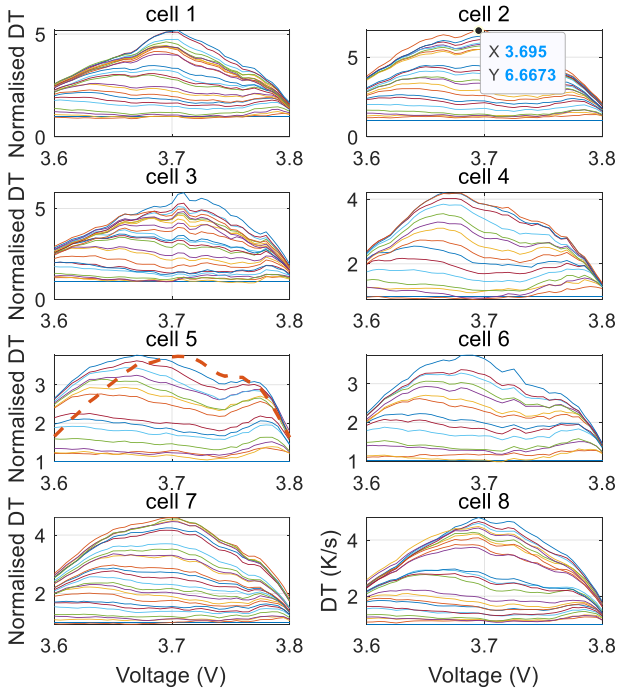

Fig. 5. Normalized DT curves of eight cells in Region II. The DT curves which rise as battery ageing are plotted every 300 cycles for brevity. The red dashed DT curve of cell 5 corresponds to the final state.

TABLE II
MAE, RMSE, AND R^2 OF SOH ESTIMATION RESULTS BEFORE AND AFTER NORMALIZATION OF EIGHT CELLS

No.	MAE		RMSE		R^2	
	Before	After	Before	After	Before	After
1	3.47%	3.34%	1.16%	1.87%	0.9766	0.9397
2	10.36%	12.59%	3.33%	5.28%	0.8445	0.6089
3	15.57%	2.32%	8.94%	1.12%	-0.4346	0.9775
4	3.33%	2.48%	1.60%	1.42%	0.9428	0.9549
5	21.03%	22.03%	3.21%	3.59%	0.7823	0.7278
6	2.40%	2.02%	0.89%	0.79%	0.9775	0.9824
7	2.69%	2.77%	0.96%	1.52%	0.9773	0.9431
8	2.97%	2.99%	1.01%	1.38%	0.9821	0.9663

and the sampling step is set to 5 mV. About 41 DT values are sampled at [3.6, 3.605, …, 3.8] V and are fed into the SVR to generate the SOH estimation results.

The estimation error is given in Fig. 4 (Unnormalized DT). The MAE, RMSE, and R^2 of the estimation results of all eight cells are summarized in Table II. As can be observed, the estimation results of cells 2, 3, and 5 suffer from large estimation error greater than 10%, 15%, and 20%, respectively. In particular, the SOH estimation error of cell 3 is always larger than 2.94%, indicating an overestimated SOH. This might be ascribed to the cell-to-cell difference, e.g., initial resistance of cell 3 might be larger. To validate this hypothesis, the DT curves are normalized before training the SVR. For the HI at the ith cycle ($i \geq 1$), the normalized HI is calculated as the element-wise division over the HI sampled at the first cycle. After normalization of the DT curves, the error falls within $\pm 2.5\%$, as indicated by the normalized DT curves in Fig. 4. The MAE and RMSE decrease from 15.57% and 8.94% to 2.32% and 1.12%, respectively, while R^2 increases from –0.4346 to 0.9775. However, large estimation errors can still be observed for cells 2 and 7, especially when SOH < 0.8. In particular, the estimation error of cell 2 dramatically increases to 10% when the SOH reaches 0.757. As shown in Fig. 5, at the end of the ageing tests, the normalized DT curve of cell 2 increases greatly and its peak value surges to 6.6673 when SOH $= 0.725$, which cannot be observed from the training dataset formed by remaining seven cells. Such extrapolation phenomenon also applies to the sharp increase in the SOH error for cell 5 when the SOH plunges at the end of the ageing test. It corresponds to a distinct DT curve which does not appear in the training dataset. This implies that the cells show different thermal behavior when the SOH plunges to 0.6, and such behavior may warn users of sudden battery failure.

Several measures can be taken to alleviate the influence of battery discrepancy on SOH estimation. On one hand, the initial inconsistency among cells should be considered. It is conducive to conduct ageing tests using batteries of different initial characteristics. It can be achieved by conducting battery clustering [39] to select batteries for ageing tests. On the other hand, a thorough offline experiment should be conducted over the wide ranges of SOH and DT in order to avoid the extrapolation during application.

2) Influence of the Voltage Range and Sampling Step: The influence of the voltage range and sampling step on the SOH estimation is investigated in this part. Three voltage ranges, namely [3.4, 3.6] V, [3.6, 3.8] V, and [3.8, 4] V in Regions I–III are investigated in combination of five sampling steps, i.e., 5, 10, 15, 20, and 25 mV. The SOH estimation errors of eight cells computed under different combinations of voltage range and sampling step are quantitatively evaluated. As can be observed from the MAE, RMSE, R^2 listed in Figs. 6–8, the

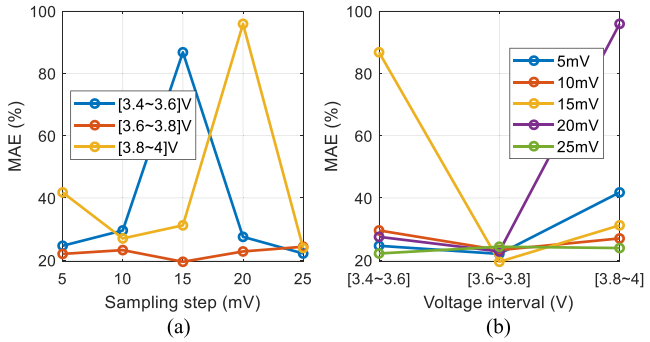

Fig. 6. MAE of SOH estimation at different combinations of voltage range and sampling step. (a) MAE versus sampling steps for different voltage intervals. (b) MAE versus voltage intervals for different sampling steps.

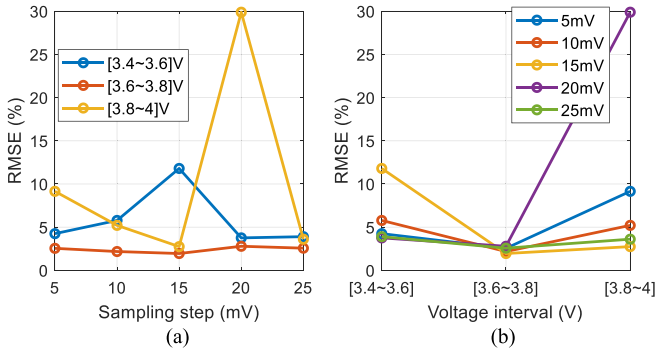

Fig. 7. RMSE of SOH estimation at different combinations of voltage range and sampling step. (a) RMSE versus sampling steps for different voltage intervals. (b) RMSE versus voltage intervals for different sampling steps.

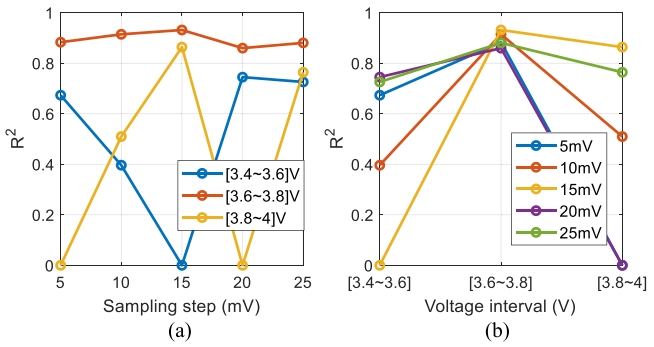

Fig. 8. R^2 of SOH estimation at different combinations of voltage range and sampling step. (a) R^2 versus sampling steps for different voltage intervals. (b) R^2 versus voltage intervals for different sampling steps. Data smaller than 0 are set to 0 for clarity in these figures.

voltage range [3.6, 3.8] V enjoys the best accuracy for all five sampling steps. The RMSE obtained from different sampling steps is less than 2.79%, while the RMSEs from [3.4, 3.6] V and [3.8, 4] V can reach as high as 11.80% and 29.89%, respectively. This is supported by the R^2 listed in Fig. 8, where their maximum values reach 0.7448, 0.9314, and 0.8636 for the ranges [3.4, 3.6] V, [3.6, 3.8] V, [3.8, 4] V, respectively. In addition, the MAE can be suppressed to 25% for [3.6, 3.8] V, which is much smaller and stabler than results from other voltage ranges. The superior

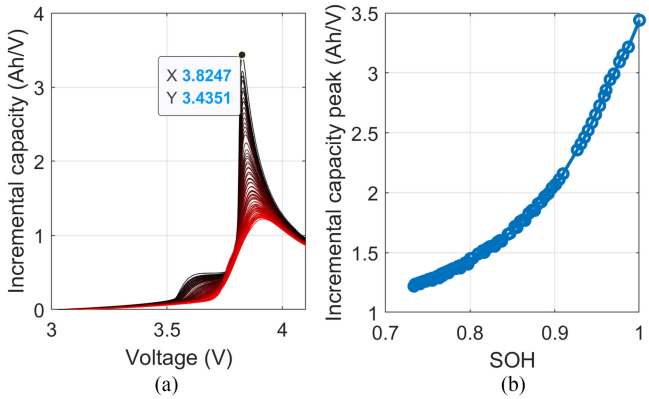

Fig. 9. (a) IC curves of cell 1. The colors range from black to red along with the increase of the cycle number. (b) Relationship between the peak height around 3.8 V and SOH for cell 1.

performance of [3.6, 3.8] V coincides with the clear trend of DT curves in Region II in Fig. 2. On the other hand, the dependency of estimation accuracy on voltage steps is rather nonlinear. A smaller sampling step does not necessarily result in a smaller SOH estimation error. This can be attributed to the fluctuations in the DT curves, as shown in Fig. 2. A smaller sampling step is more sensitive to such fluctuations. The best combination is the voltage range of [3.6, 3.8] V and the sampling step of 15 mV. In this case, the MAE and RMSE are within 19.50% and 1.95%, respectively, and the R^2 is 0.9314. Other combinations of different voltage steps and [3.6, 3.8] V show a slightly inferior performance and their discrepancy is smaller than the estimation results when other voltage ranges are adopted.

3) Comparison With the ICA Method: The proposed SOH estimation method is compared with the widely used ICA-based SOH estimation method in this part. IC curves are generated using the method reported by Tang *et al.* [18], and the results are shown in Fig. 9. A clear relationship can be observed between the height of the dominant IC peak around 3.8 V and SOH, which has been widely used for SOH estimation in different forms [16], [17]. In this part, this relationship is trained by using the identical SVR to form an ICA-based SOH estimator using peak height as the input. The performances of the ICA and DT-based estimators are compared by using the identical leave-one-out validation scheme. For the latter estimator, the voltage range and sampling step are selected to be [3.6, 3.8] V and 15 mV, respectively, and the results are shown in Fig. 10 and Table III.

As can be observed from Fig. 10 and Table III, the ICA-based SOH estimator outperforms the DT-based SOH estimator in most cases, and their maximum RMSEs are 3.51% and 3.62%, respectively. The superior accuracy of the ICA-based estimator can be attributed to stable and accurate terminal voltage sampling. Although the Oxford dataset was not intentionally designed to investigate temperature variation, the DT-based SOH estimator can still accurately estimate SOH with an RMSE less than 1.80% for six cells for which no extrapolation happens. On the other hand, the accuracy of the ICA-based estimator deteriorates for cells 2 and 5 because of the inevitable extrapolation, which agrees well with the DT-based SOH estimator.

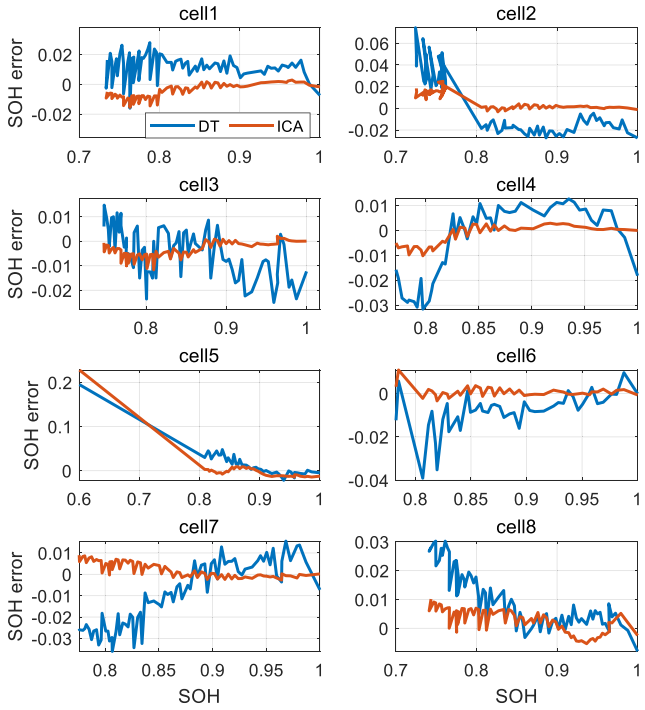

Fig. 10. Comparison of SOH estimation error between the DT and ICA-based estimators.

TABLE III
COMPARISON OF SOH ESTIMATION ERROR IN TERMS OF MAE, RMSE, AND R^2 BETWEEN DT AND ICA-BASED ESTIMATORS

No.	MAE		RMSE		R^2	
	DT	ICA	DT	ICA	DT	ICA
1	2.79%	1.55%	1.43%	0.65%	0.9647	0.9927
2	7.43%	2.49%	2.81%	0.97%	0.8896	0.9869
3	2.50%	1.16%	1.08%	0.45%	0.9792	0.9963
4	3.15%	1.01%	1.50%	0.41%	0.9500	0.9962
5	19.50%	22.81%	3.62%	3.51%	0.7240	0.7407
6	3.90%	1.08%	1.17%	0.23%	0.9602	0.9984
7	3.61%	0.90%	1.80%	0.40%	0.9211	0.9961
8	3.02%	1.01%	1.39%	0.49%	0.9659	0.9958

The DT-based SOH estimator has the MAE of 19.50% under this condition, which is 3.31% less than that of the ICA-based counterpart.

To quantitatively evaluate the computational burden, the DT and ICA-based estimators are implemented for ten times using MATLAB 2019a on a laptop (Intel Core i5-6300HQ @ 2.30 GHz, 8 GB RAM). Since the Kalman filter has been demonstrated to be easily used in a microcontroller [2], [40], its computational time is ignored. The average running time of offline training and SOH estimation of the two estimators for eight cells is reported in Table IV. Although the DT-based estimator has a vector as input, in some cases its training process can be even faster than that of the ICA-based estimator. The average training time for all eight cases is 63.59 and 86.62 s for DT and ICA-based estimators, respectively. On the other hand, the application of the offline trained estimator is usually implemented in a microcontroller [40]. After the estimator has been trained using a training dataset, the SOH estimation is conducted against the corresponding validation datasets, each

TABLE IV
COMPUTATIONAL TIME OF THE DT AND ICA-BASED ESTIMATORS

No.	Offline training time (s)		SOH estimation time (ms)	
	DT	ICA	DT	ICA
1	101.21	81.09	0.68	0.43
2	52.39	28.26	0.64	0.39
3	28.83	44.01	0.61	0.49
4	96.63	102.50	0.83	0.36
5	89.49	94.53	0.47	0.41
6	92.49	154.83	0.51	0.38
7	25.10	84.82	0.43	0.47
8	22.56	102.91	0.52	0.43

of which covers the whole life span of a cell. In this case, the ICA method is faster than the DT method, and the average time required to estimate the SOH of a cell over its whole life span is 0.42 and 0.59 ms for DT and ICA-based estimators, respectively. As each training dataset contains tens of cycles, and the computational time for one estimation is much less. Both estimators are very fast to realize SOH estimation after being trained. Accordingly, incorporating the DT-based SOH estimator in a BMS will bring little additional cost.

B. Validation on the NASA Dataset

To further validate the practicability of the proposed SOH estimation method, the proposed method is applied to the NASA dataset in this section.

The steps to extract the HIs and train the SVR algorithm are repeated. Considering the different battery specifications and ageing tests, the combinations of voltage range and sampling intervals are compared based on the leave-one-out scheme, similar to Section IV-A and the detailed comparison is not repeated here. Results show the combination of the voltage range of [3.8, 4] V and the sampling step of 10 mV has the best performance. As for the ICA method, the height of the largest IC peak is extracted as the HI and its relationship with SOH is also established using SVR. Results of the two SOH estimation methods are compared in Fig. 11 and Table V.

It can be noted that although the NASA dataset has a smaller training dataset for each validation case, the proposed method is capable of estimating SOH with the error less than 6.29% over the whole battery life. The RMSE for three cells are within 2.49% and the R^2 is higher than 0.9429. The estimation accuracy is comparable to the results of the ICA method, and can be even better for NASA-2.

C. Combination With the ICA Method

The discrepancy of estimation results between two estimators can be observed from the results of two datasets. For instance, in the case of cell 1 and NASA-2, the SOH is over- and underestimated by two methods, respectively. The discrepancy implies that two methods rely on different sources of information and combining two methods has the potential to result in a more accurate SOH estimation. To demonstrate this, the estimation results of cell 1 and NASA-2 from the two estimators are combined using the Kalman filter. In this regard, the SOH estimation

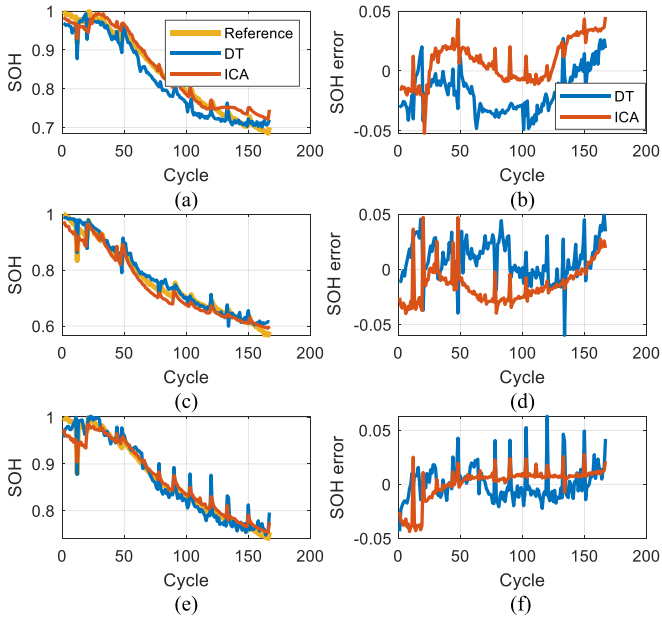

Fig. 11. SOH estimation results for the NASA dataset. (a) SOH estimation result and (b) error for NASA-1. (c) SOH estimation result and (d) error for NASA-2. (e) SOH estimation result and (f) error for NASA-3.

TABLE V
MAE, RMSE, AND R^2 OF SOH ESTIMATION RESULTS FOR THE NASA DATASET

No.	MAE		RMSE		R^2	
	DT	ICA	DT	ICA	DT	ICA
NASA-1	4.90%	5.21%	2.49%	1.94%	0.9429	0.9651
NASA-2	5.97%	4.71%	1.96%	2.16%	0.9746	0.9692
NASA-3	6.29%	4.36%	1.58%	1.53%	0.9645	0.9669

results from the two estimators are considered as measurements of the actual SOH. In addition, the SOH fade between two SOH measurements is assumed to be slight and is ignored. Then, we have the following state space:

$$\begin{cases} Q(i) = Q(i-1) + w(i-1) \\ \left[\hat{Q}_T(i)\ \hat{Q}_V(i)\right]^T = \left[1\ 1\right]^T Q(i) + v(i) \end{cases} \tag{12}$$

where $\hat{Q}_V(i)$ and $\hat{Q}_T(i)$ represent the estimation results of the from the ICA and DT-based estimation methods at the ith cycle, respectively. $Q(i)$ represents the combined estimation result. In this regard, the weights of the two methods are decided by the covariances, which affect the gain of the Kalman filter according to the equations in Table I. Qualitatively, the weights are not fixed and small covariance indicates a relatively large weight and vice versa. It should be underlined that a reasonable setting for the combination can be given by comparing the robustness and accuracy of HIs and algorithms through hardware-in-the-loop tests [40], [41]. However, to the best of the authors' knowledge, there is still no such studies. In the present work, the algorithm settings are set to be $Q_f = 0.1$, $R_f = \left[\begin{smallmatrix} 1 & 0 \\ 0 & 0.5 \end{smallmatrix}\right]$, $P(1) = 10$ based

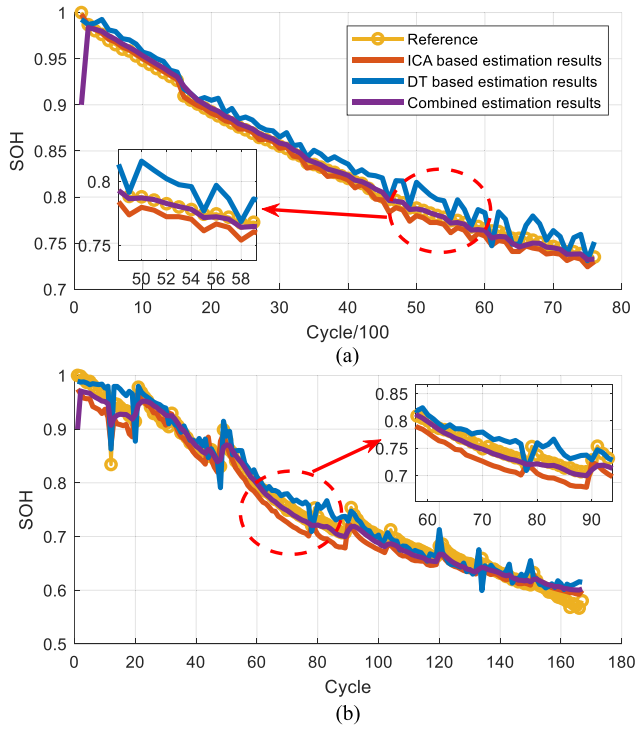

Fig. 12. Combined SOH estimation results for (a) cell 1 and (b) NASA-2.

on experience. An initial error of 10% is imposed on the combined estimation result to test the convergence.

As shown in Fig. 12, in both cases, the combined estimation result quickly converges to a small error and has a superior accuracy when the results of two individual methods show large discrepancies. This phenomenon indicates that it is promising to improve the SOH estimation accuracy of the widely used ICA-based method by combining with the proposed DT method. Besides improving the estimation accuracy, the combination is also promising to enhance the estimation robustness. Kalman filter is able to filter the random variation appears in the estimation results from the two methods, as demonstrated by Fig. 12. In addition, as two methods rely on different signals, if the ICA-based SOH estimator encounters unexpected disturbances such as sensor faults, the DT-based estimator can still provide an auxiliary SOH estimate and vice versa. The influence of error in one method can be reduced in the combined results, thanks to the combination. This can guarantee the basic performance of a BMS, and a large discrepancy between the SOH estimation results can be a criterion for fault diagnosis [42]. The only cost of adding this function into the BMS is the computational burden, as the surface temperature is usually sampled for thermal management in present BMSs. In the future, methods based on other signals, such as ultrasound [22], force [21], can also be incorporated into the combination framework to further reduce the risk of the overall failure of SOH estimation caused by sensor faults, and trigger a further fault diagnosis.

D. Further Discussions

In this article, the proposed method is validated at fixed ambient temperatures, and a combination framework has been

proposed to guarantee the overall performance of SOH estimation. As demonstrated by [28] and [29], the variation of ambient temperature can affect the performance of state estimation methods as the performance of lithium ion batteries are sensitive to ambient temperature. To guarantee the performance of the proposed method, several measures can be taken, which are as follows.

1) *Battery tests:* By conducting battery ageing and characterization tests, we can collect data about the temperature variation at different ambient temperatures [43]. Using such data as the training dataset of the SVR, we can incorporate the ambient temperature as the input, therefore, the method can be more robust against varying ambient temperature.
2) *Thermal management:* In some scenarios such as electric vehicles, a battery thermal management system is usually designed to monitor and regulate the ambient temperature. In this case, ambient temperature can be controlled to ensure the performance of the proposed method. In addition, the change in the ambient temperature can be monitored to indicate the robustness of the proposed method.
3) *Thermal models:* Another way to alleviate the influence of ambient temperature on SOH estimation is to use thermal models, which theoretically model battery heath generation and temperature rise [23]. In addition, thermal modeling is able to estimate internal temperature through identification algorithms [23]. In this way, internal temperature and electrothermal parameters such as entropy change can be extracted from surface temperature variation based on identification. The extracted internal temperature and thermal parameters are conducive to understanding battery ageing mechanisms and can be used to establish the relationship with SOH. As a model-based method, such an approach is more suitable for dynamic ambient temperature which can provide sufficient model input and output.

V. Conclusion

SOH estimation is of vital importance for the safety and performance of lithium ion batteries. Most state-of-the-art SOH estimation methods rely on the terminal voltage while neglecting other information sources. In this article, a novel SOH estimation method is proposed by extracting the health indicator from sampled surface temperature. The DT curves in a specific voltage interval are adopted for SOH estimation by combining with support vector regression.

The influence of battery discrepancy on SOH estimation is investigated, and the best combination of the voltage range and sampling step is determined. The developed SOH estimator is validated against the Oxford and NASA datasets collected from different cells under different experiments. The RMSE is within 3.62% and 2.49% for the Oxford and NASA datasets, respectively. Comparison with the popular ICA-based SOH estimation method shows the proposed SOH estimation method has high accuracy and low computational burdens. In addition, the proposed method is also able to improve the overall accuracy and robustness of SOH estimation by combining with the ICA-based method.

In the future, thermal models will be used to investigate the influence of ambient temperature on SOH estimation.

Acknowledgement

The authors would like to thank the University of Oxford and NASA for providing valuable battery degradation datasets. Jinpeng Tian would like to acknowledge the funding support from the China Scholarship Council (CSC).

References

[1] M. R. Palacin and A. de Guibert, "Why do batteries fail?" *Science*, vol. 351, no. 6273, Feb. 2016, Art. no. 1253292.
[2] Y. Zheng, M. Ouyang, X. Han, L. Lu, and J. Li, "Investigating the error sources of the online state of charge estimation methods for lithium-ion batteries in electric vehicles," *J. Power Sources*, vol. 377, pp. 161–188, Feb. 2018.
[3] X. Lin, "Theoretical analysis of battery SOC estimation errors under sensor bias and variance," *IEEE Trans. Ind. Electron.*, vol. 65, no. 9, pp. 7138–7148, Sep. 2018.
[4] B. Stiaszny, J. C. Ziegler, E. E. Krauß, M. Zhang, J. P. Schmidt, and E. Ivers-Tiffée, "Electrochemical characterization and post-mortem analysis of aged $LiMn_2O_4$-NMC/graphite lithium ion batteries part II: Calendar aging," *J. Power Sources*, vol. 258, pp. 61–75, 2014.
[5] U. Tröltzsch, O. Kanoun, and H. R. Tränkler, "Characterizing aging effects of lithium ion batteries by impedance spectroscopy," *Electrochim. Acta*, vol. 51, nos. 8/9, pp. 1664–1672, 2006.
[6] X. Zhou, Z. Pan, X. Han, L. Lu, and M. Ouyang, "An easy-to-implement multi-point impedance technique for monitoring aging of lithium ion batteries," *J. Power Sources*, vol. 417, pp. 188–192, Mar. 2019.
[7] L. Chen, Z. Lü, W. Lin, J. Li, and H. Pan, "A new state-of-health estimation method for lithium-ion batteries through the intrinsic relationship between ohmic internal resistance and capacity," *Measurement*, vol. 116, pp. 586–595, 2018.
[8] R. Xiong, J. Tian, H. Mu, and C. Wang, "A systematic model-based degradation behavior recognition and health monitoring method for lithium-ion batteries," *Appl. Energy*, vol. 207, pp. 372–383, Dec. 2017.
[9] Z. Chen, C. C. Mi, Y. Fu, J. Xu, and X. Gong, "Online battery state of health estimation based on Genetic Algorithm for electric and hybrid vehicle applications," *J. Power Sources*, vol. 240, pp. 184–192, 2013.
[10] S. Dey, B. Ayalew, and P. Pisu, "Combined estimation of state-of-charge and state-of-health of li-ion battery cells using SMO on electrochemical model," in *Proc. 13th Int. Workshop Variable Struct. Syst.*, 2014, pp. 1–6.
[11] J. Tian, R. Xiong, and Q. Yu, "Fractional-order model-based incremental capacity analysis for degradation state recognition of lithium-ion batteries," *IEEE Trans. Ind. Electron.*, vol. 66, no. 2, pp. 1576–1584, Feb. 2019.
[12] X. Hu, J. Jiang, D. Cao, and B. Egardt, "Battery health prognosis for electric vehicles using sample entropy and sparse Bayesian predictive modeling," *IEEE Trans. Ind. Electron.*, vol. 63, no. 4, pp. 2645–2656, Apr. 2016.
[13] J. Tian, R. Xiong, and W. Shen, "A review on state of health estimation for lithium ion batteries in photovoltaic systems," *eTransportation*, vol. 2, Nov. 2019, Art. no. 100028.
[14] A. Tomaszewska *et al.*, "Lithium-ion battery fast charging: A review," *eTransportation*, vol. 1, 2019, Art. no. 100011.
[15] M. Dubarry, V. Svoboda, R. Hwu, and B. Yann Liaw, "Incremental capacity analysis and close-to-equilibrium ocv measurements to quantify capacity fade in commercial rechargeable lithium batteries," *Electrochem. Solid-State Lett.*, vol. 9, no. 10, pp. A454–A457, 2006.
[16] C. Weng, Y. Cui, J. Sun, and H. Peng, "On-board state of health monitoring of lithium-ion batteries using incremental capacity analysis with support vector regression," *J. Power Sources*, vol. 235, no. 4, pp. 36–44, 2013.
[17] Y. Li *et al.*, "A quick on-line state of health estimation method for Li-ion battery with incremental capacity curves processed by Gaussian filter," *J. Power Sources*, vol. 373, pp. 40–53, 2018.
[18] X. Tang *et al.*, "A fast estimation algorithm for lithium-ion battery state of health," *J. Power Sources*, vol. 396, pp. 453–458, Aug. 2018.
[19] B. Wu, V. Yufit, Y. Merla, R. F. Martinez-Botas, N. P. Brandon, and G. J. Offer, "Differential thermal voltammetry for tracking of degradation in lithium-ion batteries," *J. Power Sources*, vol. 273, pp. 495–501, 2015.

[20] Y. Wu and A. Jossen, "Entropy-induced temperature variation as a new indicator for state of health estimation of lithium-ion cells," *Electrochim. Acta*, vol. 276, pp. 370–376, 2018.
[21] N. A. Samad, Y. Kim, J. B. Siegel, and A. G. Stefanopoulou, "Battery capacity fading estimation using a force-based incremental capacity analysis," *J. Electrochem. Soc.*, vol. 163, no. 8, pp. A1584–A1594, 2016.
[22] K. W. Knehr, T. Hodson, C. Bommier, G. Davies, A. Kim, and D. A. Steingart, "Understanding full-cell evolution and non-chemical electrode crosstalk of li-ion batteries," *Joule*, vol. 2, no. 6, pp. 1146–1159, 2018.
[23] X. Lin *et al.*, "Online parameterization of lumped thermal dynamics in cylindrical lithium ion batteries for core temperature estimation and health monitoring," *IEEE Trans. Control Syst. Technol.*, vol. 21, no. 5, pp. 1745–1755, Sep. 2013.
[24] C. Hendricks, N. Williard, S. Mathew, and M. Pecht, "A failure modes, mechanisms, and effects analysis (FMMEA) of lithium-ion batteries," *J. Power Sources*, vol. 297, pp. 113–120, 2015.
[25] F. Leng, C. M. Tan, and M. Pecht, "Effect of temperature on the aging rate of li ion battery operating above room temperature," *Sci. Rep.*, vol. 5, pp. 1–12, 2015.
[26] S. J. Drake *et al.*, "Heat generation rate measurement in a Li-ion cell at large C-rates through temperature and heat flux measurements," *J. Power Sources*, vol. 285, pp. 266–273, 2015.
[27] X. Zhang, X. Chang, Y. Shen, and Y. Xiang, "Electrochemical-electrical-thermal modeling of a pouch-type lithium ion battery: An application to optimize temperature distribution," *J. Energy Storage*, vol. 11, pp. 249–257, 2017.
[28] H. Chaoui, A. El Mejdoubi, and H. Gualous, "Online parameter identification of lithium-ion batteries with surface temperature variations," *IEEE Trans. Veh. Technol.*, vol. 66, no. 3, pp. 2000–2009, Mar. 2017.
[29] A. El Mejdoubi, A. Oukaour, H. Chaoui, H. Gualous, J. Sabor, and Y. Slamani, "State-of-charge and state-of-health lithium-ion batteries' diagnosis according to surface temperature variation," *IEEE Trans. Ind. Electron.*, vol. 63, no. 4, pp. 2391–2402, Apr. 2016.
[30] C. Birkl, "Oxford battery degradation dataset 1," Univ. Oxford, Oxford, U.K., 2017.
[31] C. Birkl, "Diagnosis and prognosis of degradation in lithium-ion batteries," DPhil thesis, , Univ. Oxford, Oxford, U.K., 2017.
[32] M. André, "The ARTEMIS European driving cycles for measuring car pollutant emissions," *Sci. Total Environ.*, vol. 334–335, pp. 73–84, 2004.
[33] B. Saha and K. Goebel, "Battery data set," *NASA Ames Prognostics Data Repository*, 2007. [Online]. Available: http://ti.arc.nasa.gov/project/prognostic-data-repository
[34] K. Maher and R. Yazami, "A study of lithium ion batteries cycle aging by thermodynamics techniques," *J. Power Sources*, vol. 247, pp. 527–533, 2014.
[35] K. Maher and R. Yazami, "Effect of overcharge on entropy and enthalpy of lithium-ion batteries," *Electrochim. Acta*, vol. 101, pp. 71–78, Jul. 2013.
[36] H. Dai, G. Zhao, M. Lin, J. Wu, and G. Zheng, "A novel estimation method for the state of health of lithium-ion battery using prior knowledge-based neural network and Markov chain," *IEEE Trans. Ind. Electron.*, vol. 66, no. 10, pp. 7706–7716, Oct. 2019.
[37] J. Meng, L. Cai, G. Luo, D. I. Stroe, and R. Teodorescu, "Lithium-ion battery state of health estimation with short-term current pulse test and support vector machine," *Microelectron. Reliab.*, vol. 88–90, pp. 1216–1220, 2018.
[38] R. R. Richardson, C. R. Birkl, M. A. Osborne, and D. A. Howey, "Gaussian process regression for in situ capacity estimation of lithium-ion batteries," *IEEE Trans. Ind. Informat.*, vol. 15, no. 1, pp. 127–138, Jan. 2019.
[39] J. Kim, J. Shin, C. Chun, and B. H. Cho, "Stable configuration of a li-ion series battery pack based on a screening process for improved voltage/SOC balancing," *IEEE Trans. Power Electron.*, vol. 27, no. 1, pp. 411–424, Jan. 2012.
[40] R. Xiong, J. Tian, W. Shen, and F. Sun, "A novel fractional order model for state of charge estimation in lithium ion batteries," *IEEE Trans. Veh. Technol.*, vol. 68, no. 5, pp. 4130–4139, May 2019.
[41] C. Chen, R. Xiong, and W. Shen, "A lithium-ion battery-in-the-loop approach to test and validate multiscale dual h infinity filters for state-of-charge and capacity estimation," *IEEE Trans. Power Electron.*, vol. 33, no. 1, pp. 332–342, Jan. 2018.
[42] R. Xiong, Q. Yu, W. Shen, C. Lin, and F. Sun, "A sensor fault diagnosis method for a lithium-ion battery pack in electric vehicles," *IEEE Trans. Power Electron.*, vol. 34, no. 10, pp. 9709–9718, Oct. 2019.
[43] Q. Wang, B. Jiang, B. Li, and Y. Yan, "A critical review of thermal management models and solutions of lithium-ion batteries for the development of pure electric vehicles," *Renewable Sustain. Energy Rev.*, vol. 64, pp. 106–128, 2016.

Jinpeng Tian (Student Member, IEEE) was born in Shandong, China, in 1994. He received the B.S. degree in vehicle engineering in 2016 from the Beijing Institute of Technology, Beijing, China, where he is currently working toward the Ph.D. degree.

He is currently a joint Ph.D. student in Swinburne University of Technology, Melbourne, Vic, Australia. His research interests include modeling and state estimation of lithium-ion batteries.

Mr. Tian was the recipient of the Best Paper Award in the International Conference on Electric and Intelligent Vehicles held in Melbourne, Australia, 2018.

Rui Xiong (Senior Member, IEEE) received the M.Sc. degree in vehicle engineering and the Ph.D. degree in mechanical engineering from the Beijing Institute of Technology, Beijing, China, in 2010 and 2014, respectively.

He conducted scientific research as a Joint Ph.D. Student at the University of Michigan, Dearborn, MI, USA, between 2012 and 2014. He is currently a Professor with the Department of Vehicle Engineering, School of Mechanical Engineering, Beijing Institute of Technology, where he was appointed as an Associate Professor from 2014. Since 2019, he has been a Visiting Professor with the Massachusetts Institute of Technology, Cambridge, MA, USA. Since 2017, he has been an Adjunct Professor with the Faculty of Science, Engineering and Technology, Swinburne University of Technology, Melbourne, Vic, Australia. His research interests include electrical/hybrid vehicles, energy storage, and battery management.

Dr. Xiong received the Highly Cited Researcher from Clarivate Analytics in 2018 and 2019. He was the recipient of the National Science Fund of China for Excellent Young Scholars in 2019, First Prize of Natural Science Award of the Ministry of Education of China in 2018, and First Prize of the Chinese Automobile Industry Science and Technology Invention Award in 2018. He serves as an Associate Editor for the IEEE ACCESS and the *SAE International Journal of Alternative Powertrains*, and on the Editorial Board for the *Applied Energy*, *eTransportation*, *and Electrical Engineering*. He is the Conference Chair of the 2017 International Symposium on Electric Vehicles (ISEV 2017), in Stockholm, Sweden, the 2018 and 2019 International Conference on Electric and Intelligent Vehicles (ICEIV 2018 and ICEIV2019), in Australia and Norway, respectively.

Weixiang Shen (Senior Member, IEEE) received the Ph.D. degree from the University of Hong Kong, Hong Kong, in 2002.

From 2002 to 2003, he was a Lecturer in Ngee Ann Polytechnic, Singapore. From 2003 to 2008, he was a Lecturer and then a Senior Lecturer with the School of Engineering, Monash University Malaysia. He then worked as a Research Fellow for one year with the School of Electrical and Electronics Engineering, Nanyang Technological University, Singapore. He is currently an Associate Professor in electrical engineering with the Faculty of Science, Engineering and Technology, Swinburne University of Technology, Melbourne, Vic, Australia. His research interests include battery charging, battery capacity estimation, battery fault diagnosis, and battery management systems for electric vehicles and integration of renewable energy sources into power grids. He has authored or coauthored more than 100 journal papers in the relevant research areas.

Dr. Shen was a General Chair of the International Conference on Energy, Ecology and Environment (ICEEE2018) held in Melbourne, Australia, 2018.